Contribution from the Department of Chemistry,
North Dakota State University, Fargo, North Dakota 58105

Influence of the Counterion Field on the Sharp-Line Excitation Spectrum of Hexacyanochromate(III)

Patrick E. Hoggard* and Kyu-Wang Lee

Received August 10, 1987

Observed splittings of 50–100 cm^{-1} in the ^2E_g, $^2T_{1g}$, and $^2T_{2g}$ states of $K_3[Cr(CN)_6]$ can be rationalized by including contributions from the cations to the ligand field potential. By the use of geometric data for the *Pcan* crystalline modification, these contributions could be represented by a value of −319 cm^{-1} for the angular overlap model (AOM) parameter e_σ for the K^+ closest to the metal ion, with a falloff as $1/R^3$ for ions at greater distances.

Introduction

$[Cr(CN)_6]^{3-}$ is an important model compound with which to test ligand field theory, and it has consequently received a good deal of attention.[1-7] In its crystalline forms it is very nearly octahedral, and the electronic spectrum should reflect this with small or zero splittings where degenerate bands are predicted in O_h symmetry. The broad transitions to the $^4T_{2g}$ and $^4T_{1g}$ states should be split into four components each by spin–orbit coupling, but negligibly in comparison to the band widths. The sharp transition to the ^2E_g state should be unsplit by spin–orbit coupling, while the sharp transitions to the $^2T_{1g}$ and $^2T_{2g}$ states would each be split into two components.[8] (Of course, in strict octahedral symmetry none of the pure electronic bands would be seen as electric dipole transitions.)

That is what the ligand field model predicts, but the experimental results are that all eight components of the $^4A_{2g} \rightarrow {}^2E_g$, $^2T_{1g}$, and $^2T_{2g}$ transitions are readily observed in absorption spectra of salts of $[Cr(CN)_6]^{3-}$.[3-5] The splittings, on the order of 50–100 cm^{-1}, are considerably larger than might be expected from the slight deviations from true octahedral symmetry of the chromophore.

Besides spin–orbit coupling, some of the effects that have been discussed in relation to sharp-line splittings in transition-metal spectra are anisotropic π-bonding by the ligands,[9] misalignment of the ligand σ-bonding orbital with the ligand–metal axis,[10] and distortions from orthoaxial ligand positions.[9] The geometry of a complex provides a basis to evaluate each of these. To the extent that the Cr–C–N bond is linear, π-bonding will be isotropic, but any deviation from a 180° angle establishes preferred directions: π-bonding perpendicular to the plane defined by the Cr, C, and N atoms will be different from that within the plane. Since the deviations from 180° are small, π-anisotropy will be ignored in this paper. For the cyanide ligand, misalignment would be extremely difficult to gauge and will also be ignored. However, the exact ligand carbon positions will be used to generate the ligand field.

One effect that has been neglected, at least quantitatively, is the contribution from the counterions. This is a particularly attractive possibility, since luminescence spectra of a number of $[Cr(CN)_6]^{3-}$ salts reveal a fairly consistent relationship between the size of the cation and the ^2E_g splitting (see Table I). Furthermore, compounds between −3 anions and +1 cations are not likely to yield high symmetry environments for either ion, increasing the possibilities for significant splittings.

Table I. ^2E_g Splittings of $[Cr(CN)_6]^{3-}$

counterion	splitting, cm^{-1}	temp, K	ref
Li^+	78	77 K	4
Na^+	58	77	4
K^+	53	77	4
K^+	48	20	5
Rb^+	49	77	4
Cs^+	54	77	4
NH_4^+	65	77	4
$As(C_6H_5)_4^+$	41	77	4
host	**splitting, cm^{-1}**	**temp, K**	**ref**
$K_3[Co(CN)_6]$	49	5	20
$Rb_3[Co(CN)_6]$	25	5	20
$Cs_3[Co(CN)_6]$	29	5	20
$Ba_3[Co(CN)_6]_2$	36	5	20
KCl	34	10	7

The means to evaluate the ligand field potential from any number of donors, by using the angular overlap model, have been discussed previously.[9] This includes, in principle, neighboring cations, although cations are usually acceptors rather than donors. In this paper we have extended the usual ligand field treatment of d^3 metal ions to include the cation environment of $[Cr(CN)_6]^{3-}$ in the potassium salt, and we evaluate its contribution to the observed splittings.

Experimental Section

$K_3[Cr(CN)_6]$ was prepared by the method of Brauer.[11] The yellow product was recrystallized three times from water by slow evaporation in the dark.

Excitation spectra of $K_3[Cr(CN)_6]$ at 13 K were measured by monitoring the zero phonon emission line at 803.5 nm. Light from an EG&G PAR Dyescan nitrogen laser-pumped dye laser was focused on microcrystalline $K_3[Cr(CN)_6]$ mounted with conductive grease on the cold head of an Air Products Displex CSA-202E cryostat. The emitted light was dispersed by a Spex Doublemate double 220-mm monochromator with 1.25-mm slits and was detected with a Hamamatsu R928 cooled photomultiplier and an EG&G PAR Model 1140A photon counter. Several laser dyes were necessary to capture the required excitation wavelength range, but no dye yielding sufficient luminescence intensity could be found for the 780–800 nm region. The spectra within each dye range were corrected for the laser intensity, but no attempt was made to normalize line intensities over all ranges. The excitation wavelength was calibrated by using four neon optogalvanic resonance points. The luminescence spectrum was measured similarly, with 0.5-mm slits.

Results and Discussion

Table II displays the frequencies of the sharp lines observed in the excitation spectrum. The eight zero phonon transitions were assigned to lines upon which a pattern of vibronic sidebands could be constructed in reasonable agreement with infrared results[12] and

(1) Schläfer, H. L.; Gausmann, H.; Wasgestian, H. F.; Zander, H. U. *Z. Phys. Chem. (Frankfurt/Main)* **1966**, *51*, 274.
(2) Condrate, R. A.; Forster, L. S. *J. Chem. Phys.* **1968**, *48*, 1514.
(3) Mukherjee, R. K.; Bera, S. C.; Bose, A. *J. Chem. Phys.* **1970**, *53*, 1287.
(4) Schläfer, H. L.; Wagener, H.; Wasgestian, F.; Herzog, G.; Ludi, A. *Ber. Bunsen-Ges. Phys. Chem.* **1971**, *75*, 878.
(5) Mukherjee, R. K.; Bera, S. C.; Bose, A. *J. Chem. Phys.* **1972**, *56*, 3720.
(6) Flint, C. D.; Greenough, P. *J. Chem. Soc., Faraday Trans. 2* **1974**, *70*, 815.
(7) Hanuza, J.; Strek, W.; Hermanowicz, K.; Jezowska-Trzebiatowska, J.; Trabjerg, I. *J. Mol. Struct.* **1986**, *144*, 141.
(8) Griffith, J. S. *The Theory of Transition Metal Ions*; Cambridge University Press: Cambridge, U.K., 1971.
(9) Hoggard, P. E. *Coord. Chem. Rev.* **1986**, *70*, 85.
(10) Gerloch, M. *Magnetism and Ligand-Field Analysis*; Cambridge University Press: Cambridge, U.K., 1983.
(11) Brauer, G. *Handbook of Preparative Inorganic Chemistry*, 2nd ed.; Academic: New York, 1965; Vol. II, p 1373.
(12) Nakagawa, I.; Shimanouchi, T. *Spectrochim. Acta*, Part *A* **1970**, *26A*, 131.

0020-1669/88/1327-2335$01.50/0

Table II. Assignment of Sharp-Line Positions in the Excitation Spectrum of $K_3[Cr(CN)_6]$ (Data in cm^{-1}, Measured from Lowest Zero Phonon Peak)

dye[a]	$\bar{\nu}$ − 12447	assignment
DOTC	387 vs	$R_2 + \tau_{1u}\ \delta(CrCN)$ (334)
	405 vs	$R_2 + \tau_{2u}\ \delta(CrCN)$ (352)
	432 s	$R_1 + \tau_{1u}\ \nu(CrC)_a$ (432)
	443 s	$R_1 + \tau_{1u}\ \nu(CrC)_b$ (443)
	484 w	$R_2 + \tau_{1u}\ \nu(CrC)_a$ (431)
	499 w	$R_2 + \tau_{1u}\ \nu(CrC)_b$ (446)
	551 m	
	654 m	T_1
	674 m	T_2
	717 m	T_3
	739 w	$R_2 + \tau_{1u}\ \delta(CrCN) + \alpha_{1g}\ \nu(CrC)$ (352)
	755 m	$R_2 + \tau_{2u}\ \delta(CrCN) + \alpha_{1g}\ \nu(CrC)$ (350)
	783 m	$R_1 + \tau_{1u}\ \nu(CrC)_a + \alpha_{1g}\ \nu(CrC)$ (351)
oxazine 725	793 m	$R_1 + \tau_{1u}\ \nu(CrC)_b + \alpha_{1g}\ \nu(CrC)$ (350)
	850 m	$R_2 + \tau_{1u}\ \nu(CrC)_b + \alpha_{1g}\ \nu(CrC)$ (351)
	897 w	
	972 w	$T_1 + \tau_{1u}\ \delta(CrCN)$ (318)
	998 s	$T_1 + \tau_{2u}\ \delta(CrCN)$ (344)
	1018 s	$T_2 + \tau_{2u}\ \delta(CrCN)$ (344)
	1048 s	$T_3 + \tau_{1u}\ \delta(CrCN)$ (331)
	1058 s	$T_3 + \tau_{2u}\ \delta(CrCN)$ (342)
	1064 s	
	1101 vs	$T_1 + \tau_{1u}\ \nu(CrC)_b$ (447)
	1110 w	$T_2 + \tau_{1u}\ \nu(CrC)_a$ (436)
	1117 m	$T_2 + \tau_{1u}\ \nu(CrC)_b$ (443)
	1164 vs	$T_3 + \tau_{1u}\ \nu(CrC)_b$ (447)
LD700 + R640	1330 vs	$T_1 + \tau_{1u}\ \delta(CrCN) + \alpha_{1g}\ \nu(CrC)$ (358)
	1338 vw	
	1355 vs	$T_1 + \tau_{2u}\ \delta(CrCN) + \alpha_{1g}\ \nu(CrC)$ (357)
	1380 w	$T_2 + \tau_{2u}\ \delta(CrCN) + \alpha_{1g}\ \nu(CrC)$ (362)
	1409 vs	$T_3 + \tau_{1u}\ \delta(CrCN) + \alpha_{1g}\ \nu(CrC)$ (361)
	1424 vw	$T_3 + \tau_{2u}\ \delta(CrCN) + \alpha_{1g}\ \nu(CrC)$ (366)
	1448 vw	$T_1 + \tau_{1u}\ \nu(CrC)_a$ (436) + $\alpha_{1g}\ \nu(CrC)$ (358)
	1457 vw	$T_1 + \tau_{1u}\ \nu(CrC)_b + \alpha_{1g}\ \nu(CrC)$ (356)
	1465 vw	$T_2 + \tau_{1u}\ \nu(CrC)_a + \alpha_{1g}\ \nu(CrC)$ (355)
	1472 vw	$T_2 + \tau_{1u}\ \nu(CrC)_b + \alpha_{1g}\ \nu(CrC)$ (355)
	1480 vw	
	1520 vs	$T_3 + \tau_{1u}\ \nu(CrC) + \alpha_{1g}\ \nu(CrC)$ (356)
	1692 w	$T_1 + \tau_{1u}\ \delta(CrCN) + 2\alpha_{1g}\ \nu(CrC)$ (360)
	1717 w	$T_1 + \tau_{2u}\ \delta(CrCN) + 2\alpha_{1g}\ \nu(CrC)$ (360)
	1774 w	$T_3 + \tau_{1u}\ \delta(CrCN) + 2\alpha_{1g}\ \nu(CrC)$ (363)
	1820 w	$T_1 + \tau_{1u}\ \nu(CrC)_b + 2\alpha_{1g}\ \nu(CrC)$ (360)
	1838 w	$T_2 + \tau_{1u}\ \nu(CrC)_b + 2\alpha_{1g}\ \nu(CrC)$ (361)
	1888 w	$T_3 + \tau_{1u}\ \nu(CrC)_b + 2\alpha_{1g}\ \nu(CrC)$ (362)
	2060 vw	
	2126 vw	$R_1 + \tau_{1u}\ \nu(CN)$ (2126)
	2172 w	$R_2 + \tau_{1u}\ \nu(CN)$ (2119)
DCM	2739 m	
	2752 vs	$T_1 + \tau_{1u}\ \nu(CN)$ (2098)
	2802 vs	$T_2 + \tau_{1u}\ \nu(CN)$ (2128)
	2814 m	$T_3 + \tau_{1u}\ \nu(CN)$ (2097)
	3100 w	$T_1 + \tau_{1u}\ \nu(CN) + \alpha_{1g}\ \nu(CrC)$ (348)
	3155 w	$T_2 + \tau_{1u}\ \nu(CN) + \alpha_{1g}\ \nu(CrC)$ (353)
Kiton Red	4153 m	
	4263 vs	$R_1 + \tau_{1u}\ \nu(CN) + \alpha_{1g}\ \nu(CN)$ (2137)
	4317 m	$R_2 + \tau_{1u}\ \nu(CN) + \alpha_{1g}\ \nu(CN)$ (2145)
Coumarin 540A	5941 s	B_1
	5988 vs	B_2
	6040 s	B_3
	6276 m	$B_1 + \tau_{1u}\ \delta(CrCN)$ (335)
	6290 m	$B_1 + \tau_{2u}\ \delta(CrCN)$ (349)
	6333 s	$B_2 + \tau_{1u}\ \delta(CrCN)$ (345)
	6339 w	$B_2 + \tau_{2u}\ \delta(CrCN)$ (351)
	6380 s	$B_3 + \tau_{1u}\ \delta(CrCN)$ (340)
	6392 w	$B_3 + \tau_{2u}\ \delta(CrCN)$ (352); $B_1 + \tau_{1u}\ \nu(CrC)_b$ (451)
	6440 w	$B_2 + \tau_{1u}\ \nu(CrC)_b$ (452)
Coumarin 500	6480 vw	$B_3 + \tau_{1u}\ \nu(CrC)_b$ (440)
	6508 m	
	6630 m	$B_1 + \tau_{1u}\ \delta(CrCN) + \alpha_{1g}\ \nu(CrC)$ (354)
	6665 w	$B_2 + \tau_{1u}\ \delta(CrCN) + \alpha_{1g}\ \nu(CrC)$ (354)
	6763 vs	$B_2 + \tau_{1u}\ \nu(CrC)_a$ (430?) + $\alpha_{1g}\ \nu(CrC)$ (345)
	6859 vw	
	7107 vs	$B_2 + \tau_{1u}\ \nu(CrC)_a$ (430?) + $2\alpha_{1g}\ \nu(CrC)$ (345)
	7481 s	
	7504 w	

[a] Dye names are those of Exciton Chemical Co.

with each other. The ^2E_g energies were taken from the luminescence spectrum. These assignments agree with those of Bose from absorption spectra.[3,5]

A major part of the vibronic structure can be built up from just five promoting modes (two Cr–C stretching modes, both τ_{1u}, but split due to the lower than octahedral symmetry; τ_{1u} and τ_{2u} Cr–C–N bending modes; a C–N stretching mode) and one accepting (progression-forming) mode, an α_{1g} Cr–C stretching motion. These constitute only a few of the vibronically active modes that have been identified in a high-resolution luminescence spectrum of $[Cr(CN)_6]^{3-}$ diluted in a $K_3[Co(CN)_6]$ host.[4] The sequence of false origins is found with reasonable regularity on all eight 0–0 transitions, with little variation in frequency, and at least one line in the progression on the $\alpha_{1g}\ \nu(CrC)$ mode is seen for most of these false origins. The observed peaks that can be assigned in this manner are so described in Table II.

An earlier paper[9] described how the exact ligand angular positions could be used to generate the ligand field potential matrix, $\langle d_i|V|d_j\rangle$. Thus the slight deviations of the cyanide carbons from octahedral coordination, which amount to about 1.0° at most,[13,14] can be treated within the AOM. The Cr–C–N angles are all near 178°, so in principle anisotropic π-bonding is occurring. This could be accounted for in the AOM by replacing the π-destabilization parameter e_π by two parameters, $e_{\pi\perp}$ and $e_{\pi\parallel}$, to be applied in the directions perpendicular and parallel to the Cr–C–N plane, respectively. Anisotropic π-bonding may indeed contribute to the sharp-line splittings, but the Cr–C–N bonds are so nearly linear that we felt an additional adjustable parameter could not be justified.

In addition to the ligand field potential, the calculation we have used[9] takes into account interelectronic repulsion, through the Racah parameters B and C and a Trees correction parameter α,

Table III. Observed and Calculated Zero Phonon Frequencies (in cm^{-1}) for the Intraconfigurational Transitions in $K_3[Cr(CN)_6]$[a]

	expt	calcd[b]	calcd[c]	calcd[d]
^2E_g	12447	12464	12479	12481
	12500	12475	12500	12491
$^2T_{1g}$	13101	13065	13083	13090
	13121	13082	13120	13127
	13164	13112	13154	13137
$^2T_{2g}$	18388	18349	18385	18376
	18435	18433	18433	18432
	18487	18547	18489	18504
$^4T_{2g}$	26600[e]	26200	26200[f]	26180
$^4T_{1g}$	32500[e]	32770	32860[g]	32870

[a] Transitions to quartet states used in the fitting procedure are also shown. The propagated error for each parameter is given in parentheses. [b] *Pcan* structure, cation field ignored: $3e_{\sigma C} - 4e_{\pi C}$ = 27387 (25), $e_{\pi C}$ = −1410 (35), ($e_{\sigma C}$ = 7249), B = 745 (1), C = 1861 (3), ζ = 0 (45), α (Trees parameter) = 195(1). [c] *Pcan* structure, field from 14 nearest cations using eq 6: $3e_{\sigma C} - 4e_{\pi C}$ = 27549 (25), $e_{\pi C}$ = 603 (515) ($e_{\sigma C}$ = 9987), $e_{\sigma K}$ = −319 (8), B = 744 (2), C = 1842 (3), ζ = 154 (4), α = 212 (1). [d] *P*$\bar{1}$ structure (one site), field from 14 nearest cations using eq 6: $3e_{\sigma C} - 4e_{\pi C}$ = 27702 (25), $e_{\pi C}$ = −1407 (132) ($e_{\sigma C}$ = 7340), $e_{\sigma K}$ = −201 (6), B = 744 (1), C = 1852 (3), ζ = 1 (724), α = 203 (1). [e] 143 K spectrum in ethylene glycol/water.[19] [f] Calculated component energies: 25961, 25971, 26093, 26104, 26610, 26611. [g] Calculated component energies: 32674, 32677, 32850, 32851, 33045, 33046.

(13) Jagner, S.; Ljungstrom, E.; Vannerberg, N.-G. *Acta Chem. Scand. Ser. A* **1974**, *28A*, 623.
(14) Figgis, B. N.; Reynolds, P. A.; Williams, G. A. *Acta Crystallogr., Sect. B: Struct. Crystallogr. Cryst. Chem.* **1981**, *B37*, 504.

Table IV. Cartesian Coordinates of Coordinated Carbon Atoms and Nearest K^+ Ions in the *Pcan*[13] Structure and One Site in the $P\bar{1}$[14] Structure of $K_3[Cr(CN)_6]$ (in Å Relative to Cr at the Origin)

	Pcan				$P\bar{1}$			
atom	*x*	*y*	*z*	dist	*x*	*y*	*z*	dist
C1	0.005	−2.057	0.019	2.057	−0.061	−2.079	0.014	2.079
C2	−0.004	−0.018	2.057	2.057	−0.051	−0.022	2.095	2.096
C3	2.075	−0.012	−0.015	2.075	2.052	−0.003	0.029	2.053
C4	−2.075	0.014	0.013	2.075	−2.098	0.020	0.039	2.099
C5	−0.024	2.100	0.012	2.100	−0.084	2.066	0.037	2.068
C6	0.023	−0.013	−2.100	2.100	−0.039	−0.045	−2.053	2.054
K1	−0.001	2.985	−2.987	4.223	0.035	2.879	−2.990	4.151
K2	0.001	−3.042	3.043	4.303	−0.055	−3.090	2.991	4.301
K3	−1.129	−3.062	−3.044	4.463	−1.226	−3.003	−2.969	4.398
K4	1.129	3.046	3.060	4.463	0.811	2.986	3.054	4.347
K5	−3.660	−0.050	2.949	4.701	−3.391	0.083	3.094	4.591
K6	3.661	−2.948	0.050	4.701	4.071	−2.723	0.390	4.914
K7	3.990	0.173	−2.857	4.910	4.335	0.306	−2.554	5.041
K8	−3.991	2.856	−0.173	4.911	−3.477	3.041	0.044	4.620
K9	4.814	1.540	1.594	5.300	4.637	1.676	1.792	5.246
K10	−4.814	−1.597	−1.538	5.300	−4.931	−1.442	−1.462	5.341
K11	0.799	5.952	−0.062	6.006	0.724	5.944	0.004	5.988
K12	−0.801	0.059	−5.952	6.006	−0.963	0.025	−5.913	5.991
K13	0.801	−0.075	5.968	6.022	0.635	−0.025	5.985	6.019
K14	−0.799	−5.968	0.078	6.022	−1.052	−5.943	0.068	6.036

and spin–orbit coupling, by the standard parameter ζ. Eigenvalues and eigenfunctions were determined by diagonalizing the full 120 × 120 d^3 secular determinant. An optimized fit to Bose's experimental data was reported earlier for strict O_h geometry,[9] but of course, the degeneracies are not lifted thereby. The second column of Table III shows the results of an optimization with the same model, using the actual carbon positions rather than idealized octahedral geometry.

The optimization procedure[9] attempted to fit both the experimental frequencies and the splittings within octahedral terms. The function minimized was

$$F = \sum(\Delta Q)^2 + 100\sum(\Delta D)^2 + 1000\sum(\Delta S)^2 \qquad (1)$$

Here ΔQ, ΔD, and ΔS represent the difference between experimental and calculated quartet energies, doublet energies, and splittings, respectively. Only the splittings between the highest and lowest levels of the ^2T states were included in F. The calculated quartet transition energies of Table III are the averages over the 12 components of the ^4T states.

In this instance the splittings do not vary much with any of the parameters. The interelectronic repulsion parameters have in general almost no effect on the splittings. Spin–orbit coupling is responsible for some splitting, but a large alteration in the value of the spin–orbit coupling constant is required to produce noticeable changes, because the geometric asymmetry is the dominant factor. The two angular overlap parameters, e_σ and e_π, are nearly redundant, since $3e_\sigma$–$4e_\pi$ is essentially fixed in O_h symmetry as long as the π-interaction is isotropic. The large negative value for $e_{\pi C}$ used to generate the data in the second column of Table III reflects a futile effort by the optimization procedure to increase the splittings of the ^2E_g and $^2T_{1g}$ states. What is surprising about the data in the second column are the large splittings within the $^2T_{2g}$ term—larger even than the experimental values.

The inability to fit the sharp-line electronic data at all satisfactorily for one of the most nearly ideal cases might be taken to mean that ligand field theory is simply unable to make predictions accurate to within tens of reciprocal centimeters, nor by implication treat sharp-line electronic bands at all. There is one effect that has been left out, however, and that is the asymmetry generated by the cations. These make up a second "coordination sphere" that can be considered to perturb the d orbitals of the metal ion, possibly as point charges in classical crystal field theory.

There are two known structures for $K_3[Cr(CN)_6]$, an orthorhombic *Pcan* structure at room temperature[13] and a $P\bar{1}$ structure at 4 K.[14] In the latter there are two distinct chromium sites. In spite of the loss of symmetry, the chromium environment in the $P\bar{1}$ structure is similar to that in the *Pcan* structure. The extent of the atom translations can be seen in Table IV, in which cartesian coordinates for the nearest 14 potassium ions are given, relative to the chromium atom, for the *Pcan* geometry and one site of the $P\bar{1}$ structure. The coordinate system for Table IV has been chosen to maximize the overlap of the six ligand carbon positions with the cartesian axes.

In the *Pcan* structure, there is somewhat more symmetry to the cation positions than meets the eye. The chromium atom is on a special position, such that any atom on a general position will have an inversion partner relative to the chromium. K1 and K2 are also on special positions and have no partners. The Cr may be thought of as imbedded in a layer of potassium ions, and is almost exactly coplanar with K1–K4 and K11–K14. The remaining six K^+ ions form triangles from the layers above and below. K1–K4 form a square (actually a near rhombus) around the Cr, while K11–K14 form another square displaced 45° from the closer one.

With no large gap in Cr–K distances, it is difficult to decide just how large to choose the K^+ coordination sphere. In our calculations we have used the 14-ion coordination sphere shown in Table IV. The next closest K^+ ions are over an angstrom further away.

Radial Dependence of the Angular Overlap Parameters. The contribution of each K^+ to the ligand field potential can be evaluated by the usual angular overlap methods.[9,15] The d orbitals are rotated so that the d_{z^2} orbital points directly at the ion. Interaction with the ion raises the energy of the rotated d_{z^2} orbital by e_σ and the rotated d_{xz} and d_{yz} orbitals by e_π (but for a positively charged ion e_σ and e_π can ordinarily be expected to be negative and the d orbital energies will be lowered). Then the d_{z^2} orbital is rotated back, spreading the interaction among all five of the original d orbitals and generating a contribution to the $\langle d_i|V|d_j\rangle$ matrix. Because of the wide variation in Cr-K distances, however, e_σ and e_π for K^+ cannot be considered constant. Their variation with distance must be accounted for.

Schäffer has analyzed the equivalence of the radial parameters in the AOM and an additive classical crystal field formalism[16]

$$e_\sigma = {}^4/_7 I_2 + {}^5/_{21} I_4 \qquad e_\pi = {}^3/_7 I_2 - {}^5/_{21} I_4 \qquad (2)$$

I_2 and I_4 represent radial integrals over the $L = 2$ and $L = 4$ terms in the expansion of the potential function for an electron in the field of a charge from a single ligand.[17] Integrals over the global potential depend also on geometric factors from all the ligands together. For example, the ligand field splitting parameter Δ (=$3e_\sigma$

(15) Schäffer, C. E. *Struct. Bonding (Berlin)* **1968**, *5*, 68.
(16) Schäffer, C. E. *Struct. Bonding (Berlin)* **1973**, *14*, 69.
(17) Schmidtke, H.-H. *Quantenchemie*; VCH Verlag: Weinheim, FRG, 1987; p 264.

$- 4e_\pi$) in an exactly octahedral complex depends on I_4 alone.

The electrostatic model provides an explicit means to quantify the radial dependence of the cation field, since the I_2 and I_4 integrals contain R^3 and R^5, respectively, in the denominators (R is the metal–ligand distance). If I_2 and I_4 do decay as R^{-3} and R^{-5}, it is reasonable to assume, for purposes of this calculation, that I_4 is negligibly small at cation distances (>4.15 Å). Then the radial dependence can be expressed as

$$I_2 = I_2^0(R_0/R)^3 \tag{3}$$

where I_2^0 is the value of I_2 at the reference distance R_0. From eq 2 we then have

$$e_\sigma = {}^4/_7 I_2 \qquad e_\pi = {}^3/_7 I_2 \tag{4}$$

Thereby the field from the cations can be incorporated into the $\langle d_i|V|d_j\rangle$ matrix in the same manner as that from the six ligands, with the single adjustable parameter $I_2^0(K^+)$.

Although this approach represents a natural extension of the classical crystal field model to include the field from the counterions, assumed to be point charges, the form of the radial dependence may nevertheless not be correct. Experimental values of the radial integrals have never been satisfactorily calculated by means of the electrostatic model. Thus experimentally determined values for I_2 and I_4 may not vary as R^{-3} or R^{-5} at all.

In fact, it may be better to instead assume a particular behavior for the AOM parameters e_σ and e_π. Since they are intended to reflect the destabilization of the metal d orbitals through overlap of σ- and π-symmetry orbitals, we may assume that this overlap and the values of e_σ and e_π decay monotonically to zero. This contradicts directly the predictions of the electrostatic model, whereby e_π would in many cases (particularly when e_π at short distances was small or negative) *increase* at large R, as it approached a value of $0.75e_\sigma$.

In a second approach to the radial dependence problem, we will assume that the functional form of eq 2 is maintained insofar as e_σ and e_π are related to distance but that I_2 and I_4 are not constrained to vary as R^{-3} and R^{-5} but instead are determined at any distance R from e_σ and e_π. The suggested functional form is

$$e_\sigma = aR^{-3} + bR^{-5} \tag{5}$$

An identical equation would apply for e_π; however, we will assume for computational simplicity that e_π is negligible at the distances involved. We assume further that at these distances the R^{-5} term can be neglected. The radial dependence is then expressed, analogously to eq 3, as

$$e_\sigma = e_\sigma^0(R_0/R)^3 \tag{6}$$

For this approach, typical e_σ values for K^+ ions at 4.2 Å will be seen to have a magnitude around 300 cm^{-1}, which reflects a more rapid than third power falloff with R, compared with typical values for ligands at about 2 Å of around 7000 cm^{-1}. However, at 2 Å not only would the R^{-5} terms be more important, but covalent effects and electron cloud repulsion would bring about a more complicated radial dependence than that depicted in eq 5.

Effects of the Cation Field. Optimizations to the experimental data in Table III were performed by using both eq 3 and eq 6 to add in the cation field, minimizing the function in eq 1. For the pure electrostatic treatment (eq 3), no improvement in the fit could be obtained when I_2^0 was restricted to negative values, as should be the case for a perturbation by a positive ion (positive values did improve the fit, optimizing at I_2^0 = 1400 cm^{-1}). This approach was not pursued further.

Modeling the cation field in terms of a monotonically decreasing AOM parameter $e_{\sigma K}$ did yield a marked improvement in the fit for negative values of $e_{\sigma K}$. Figure 1 illustrates the calculated effects on the doublet transition energies from the field generated by the 14 nearest cations in the *Pcan* crystal geometry. The parameter $e_{\sigma K}$ is the value for the nearest K^+ ion, the rest being reduced by the factor $(R_0/R)^3$. It can be seen that an appropriate choice of field strength can lead either to the observed ^2E_g splitting near 50 cm^{-1} or to a reduction in the splitting of the $^2T_{2g}$ state to the

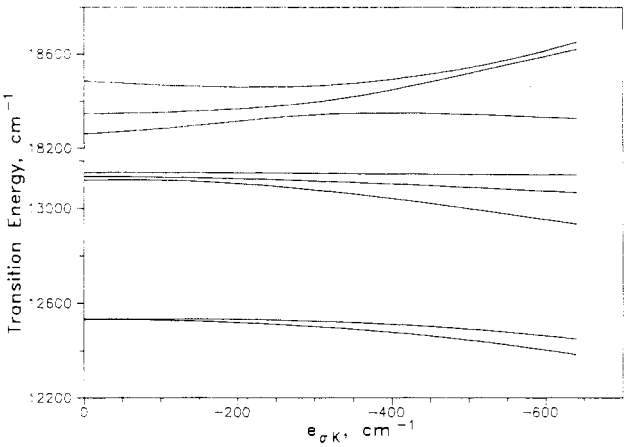

Figure 1. Calculated variaton of transition energies to the ^2E_g, $^2T_{1g}$, and $^2T_{2g}$ levels of $K_3[Cr(CN)_6]$ as a function of the cation field, represented by $e_{\sigma K}$. Conditions: *Pcan* geometry, $e_{\sigma C}$ = 10024, $e_{\pi C}$ = 592, B = 729, C = 1857, α (Trees parameter) = 223, ζ = 199 (all in cm^{-1}).

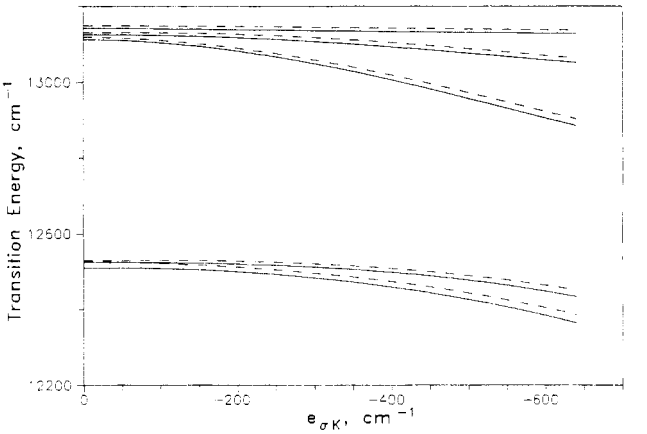

Figure 2. Calculated variation of transition energies to the ^2E_g and $^2T_{1g}$ levels of $K_3[Cr(CN)_6]$ as a function of the cation field, represented by $e_{\sigma K}$. Solid and dotted lines signify the two distinct sites of the $P\bar{1}$ structure. All parameters were identical with those in Figure 1.

observed 100 cm^{-1}, though not at the same value of $e_{\sigma K}$. For the $P\bar{1}$ structure the $^2T_{2g}$ splitting cannot be reduced to 100 cm^{-1} at any value of e_σ for either chromium site. Within the model used here, the two $P\bar{1}$ chromium sites appear to be quite similar. Figure 2 shows calculated transition energies to ^2E_g and $^2T_{1g}$ levels for both sites as a function of the cation field strength. The observed sharp-line splittings are too large to be ascribed to the two sites of the $P\bar{1}$ structure.

The optimization results are listed in Table III for both the *Pcan* and the $P\bar{1}$ geometries. The error limits for the best-fit parameters are those resulting just from the error propagated from average experimental uncertainties of 30 cm^{-1} for the quartets, 3 cm^{-1} for the doublets, and 1 cm^{-1} for the term splittings. Actual error limits, which would recognize sizable tolerances in the calculated transition energies due to inadequacies in the model, would be considerably larger. In particular, the individual values of $e_{\sigma C}$ and $e_{\pi C}$ are almost meaningless. The environment is close to octahedral, in which as long as $\Delta = 3e_\sigma - 4e_\pi$ were held constant, e_σ or e_π could be varied at will with no change in the transition energies. In the actual chromium environment the redundancy is lifted, but nevertheless a change in either e_σ or e_π can almost be compensated by a change in the other. During the optimization, therefore, we used $(3e_\sigma - 4e_\pi)$ and e_π as the two AOM ligand parameters to be varied, but added a penalty function to eq 1 to restrict e_π approximately to the range from −1400 to +600 cm^{-1}, based on an expected value of around −400 cm^{-1}.[18]

(18) Vanquickenborne, L. G.; Ceulemans, A. *J. Am. Chem. Soc.* **1977**, *99*, 2208.
(19) Alexander, J. J.; Gray, H. B. *J. Am. Chem. Soc.* **1968**, *90*, 4260.

Thus neither e_σ nor e_π for CN^- can be even approximated from this treatment. It is also unrealistic to accept the best-fit ζ values, even when the propagated error turns out to be small, because changes in ζ induce smaller changes in the transition energies than would such factors as the inclusion of additional K^+ (or $[Cr(CN)_6]^{3-}$) ions in the model.

The value of the Trees parameter, 211 cm^{-1} using the *Pcan* structure, appears large by comparison with the 70-cm^{-1} value for the free Cr^{3+} ion.[8] Smaller values of the Trees parameter place the $^2T_{2g}$ levels too high in energy when B and C are chosen to fit the quartets and the ^2E_g and $^2T_{1g}$ levels.

The fit to the experimental energies is definitely better for the *Pcan* geometry, but the model includes too many approximations to justify a prediction that this is the structure at 13 K, the temperature at which the excitation spectrum was measured. With either the *Pcan* or $P\bar{1}$ geometry, including a cation field of reasonable magnitude yields a better fit to experiment than no field at all. It is not obvious that this should be so, because at zero cation field the calculated $^2T_{2g}$ splitting is too large, while the ^2E_g splitting is too small. If increasing the field increased all splittings monotonically, as many perturbations might be expected to do, the fit would be worse at any value of $e_{\sigma K}$.

We conclude that it is appropriate to include in any ligand field calculation a field from the counterions. This field appears to be better represented by an AOM parameter $e_{\sigma K}$ decreasing with R^3 than by an electrostatic parameter I_2 varying in the same manner. The appropriate magnitude of e_σ is ±200-400 cm^{-1} (for ions ~4 Å from the metal ion). Whether it is necessary to include the counterion field depends on the symmetry of the counterion sphere. If it is nearly cubic, there will be negligible contributions to the sharp-line splittings, and it would not matter whether it were included or not. The case of a ±3 chromophore with ±1 counterions, as represented here, is very likely to produce a counterion environment of lower symmetry, requiring explicit consideration of that environment.

Acknowledgment. We thank the donors of the Petroleum Research Fund, administered by the American Chemical Society, for support of this research. This work was also supported in part by the National Science Foundation under Grant RII8610675. We also thank Prof. Claus Schäffer for helpful comments.

Registry No. $K_3[Cr(CN)_6]$, 13601-11-1.

(20) Flint, C. D.; Palacio, D. J. D. *J. Chem. Soc. Faraday Trans. 2* **1977**, *73*, 649.

Contribution from the Department of Chemistry, Harvard University, Cambridge, Massachusetts 02138

Hexanuclear Iron-Sulfur Basket Clusters: Topological Isomers of Prismanes. Synthesis, Structure, and Reactions

Barry S. Snyder and R. H. Holm*

Received December 11, 1987

The new set of cluster molecules $Fe_6S_6(PEt_3)_4X_2$ (X = Cl^- (**1**), Br^-, I^-) has been prepared by the reaction of $Fe(PEt_3)_2X_2$ (**2**) with (i) $(Me_3Si)_2S$ or Li_2S in THF, (ii) the cubane clusters $[Fe_4S_4X_4]^{2-}$ in acetonitrile, and (iii) the prismane clusters $[Fe_6S_6X_6]^{3-}$ in acetonitrile. Also prepared by similar means were $Fe_6S_6(PMe_3)_4Cl_2$, $Fe_6Se_6(PEt_3)_4Cl_2$, and $Fe_6S_6(P\text{-}n\text{-}Bu_3)_4Cl_2$ (**3**). The compounds were obtained as black crystalline solids, usually in purified yields of 50-65%. Precursor complex **2** (X = Br^-) was isolated as pale yellow crystals with monoclinic space group *Pn*, a = 7.316 (1) Å, b = 12.316 (2) Å, c = 11.356 (2) Å, β = 97.15 (2)°, and Z = 2. The expected (distorted) tetrahedral structure was confirmed, with a notably open Br-Fe-Br angle (121.9 (1)°) presumably set by steric interactions. This angle is one of the largest in the tetrahedral series $M(PR_3)_2X_2$, all of which thus far have X-M-X angles ≥105°; no previous structural data have been reported for type **2** complexes. Compound **3** crystallizes in tetragonal space group $I4_1$ with a = 33.78 (1) Å, c = 12.362 (7) Å, and Z = 8. It contains a $[Fe_6(\mu_2\text{-}S)(\mu_3\text{-}S)_4(\mu_4\text{-}S)]^{2+}$ core, formally including 2 Fe(III) + 4 Fe(II), and is built by the fusion of six nonplanar Fe_2S_2 rhombs to form an open basket with a bridging group Fe-(μ_2-S)-Fe of bond angle 75.5° as the "handle". The core has idealized C_{2v} symmetry with the 2-fold axis containing the μ_2-S and μ_4-S atoms. Each Fe atom is four-coordinate; the two FeS_3Cl sites have trigonally distorted tetrahedral geometry whereas the four FeS_3P sites resemble very distorted trigonal pyramids with the Fe atoms only ca. 0.11 Å above the S_3 planes and expanded S-Fe-S angles, one at each site (mean 127.5°), which form edges of the basket and handle in the form of two chairlike Fe_3S_3 rings or "open faces". A simple conceptual relationship among 6-Fe core structures is presented as a scheme wherein different cores are transformed by formal addition (or subtraction) of Fe and S atoms. Arguments based on electrochemical properties are provided to show that basket and prismane ($[Fe_6(\mu_3\text{-}S)_6]$) cores do not interconvert even in the same oxidation level and are therefore topological isomers. The typical cluster **1** exhibits a versatile reaction chemistry that includes unique transformations that result in core conversions. In addition to being formed from $[Fe_6S_6Cl_6]^{3-}$ (**4**) in a reductive-substitution reaction and from $[Fe_4S_4Cl_4]^{2-}$ (**5**) in a process of core enlargement and reductive substitution, it is also spontaneously generated in solution from $Fe_7S_6(PEt_3)_4Cl_3$. Further, in the presence of sulfur and chloride, the phosphines of **1** are removed in the form of Et_3PS in high yield. In acetone solution in the presence of $(Me_4N)Cl$, $(Me_4N)_2$[**5**] was isolated, whereas the use of (PPN)Cl resulted in isolation of the $(PPN)^+$ salts of **4** and $[Fe_2S_2(S_5)_2]^{2-}$, the latter in low yield. $(PPN)_3$[**4**] could be identified securely only by X-ray crystallography. This compound crystallizes in monoclinic space group $C2/c$ with a = 28.929 (8) Å, b = 15.296 (5) Å, c = 28.898 (6) Å, β = 122.39 (2)°, and Z = 4. The anion has a slightly distorted hexagonal prismatic structure with dimensions comparable to those found previously for another salt. In these conversions 85% of the Fe content of **1** is accounted for in the products. The basket and prismane Fe_6S_6 cores are the only open or closed polyhedral cores of this stoichiometry. The open faces of the prismane can be capped by certain metal fragments. These faces of the basket core have the same potential, but their less regular shape and longer S···S separations (3.93-4.10 Å) presumably will require core structural adjustment in the event of formation of a stable capped product.

Introduction

The continuing evolution of iron-sulfur chemistry has resulted in the synthesis of new types of clusters with nuclearities exceeding that of the familiar, biologically relevant cubane-type species containing the $[Fe_4(\mu_3\text{-}S)_4]^{2+,+}$ cores.[1] The first examples of such higher nuclearity clusters in this field were $[Fe_6S_9(SR)_2]^{4-,2-}$[5] containing the rather complicated $[Fe_6(\mu_4\text{-}S)(\mu_3\text{-}S)_2(\mu_2\text{-}S)_6]^{2-}$ core

(1) Berg, J. M.; Holm, R. H. In *Metal Ions in Biology*; Spiro, T. G., Ed.; Interscience: New York, 1982; Vol. 4, Chapter 1.

0020-1669/88/1327-2339$01.50/0